



3D geo-cellular modeling for Oligocene reservoirs: a marginal field in offshore Vietnam

Hung Vo Thanh¹ · Kang-Kun Lee¹

Received: 27 July 2021 / Accepted: 11 September 2021
© The Author(s) 2021

Abstract

This study focuses on constructing a 3D geo-cellular model by using well-log data and other geological information to enable a deep investigation of the reservoir characteristics and estimation of the hydrocarbon potential in the clastic reservoir of the marginal field in offshore Vietnam. In this study, Petrel software was adopted for geostatistical modeling. First, a sequential indicator simulation (SIS) was adopted for facies modeling. Next, sequential Gaussian simulation (SGS) and co-kriging approaches were utilized for petrophysical modeling. Furthermore, the results of the petrophysical models were verified by a quality control process before determining the in-place oil for each reservoir in the field. Multiple geological realizations were generated to reduce the geological uncertainty of the model assessment for the facies and porosity model. The most consistent one would then be the best candidate for further evaluation. The porosity distribution ranged from 9 to 22%. The original oil place of clastic reservoirs in the marginal field was 50.28 MMbbl. Ultimately, this research found that the marginal field could be considered a potential candidate for future oil and gas development in offshore Vietnam.

Keywords 3D geo-cellular · Marginal field · Offshore Vietnam · Petrophysical modeling

Abbreviations

BRV	Volume reservoir of rock
RQI	Reservoir quality index
Bo	Volume factor
NTG	Ratio between effective thickness and total thickness
J _{fu}	J _{function}
OIIP	Oil initial in place
PHIE	Effective porosity
Sw	Water saturation
C	Covert coefficient from m ³ to bbl
OWC _H	Oil water contact height
Pc	Capillary pressure
Vcl	Volume of clay
Pow	Power
Perm _{E10}	E10 permeability
Perm _{E20}	E20 permeability

Introduction

The Cuu Long Basin is a well-known source for exploring and producing hydrocarbons in Vietnam (Thanh et al. 2019). However, oil and gas have been extracted from this basin for a long time. As a result, the large reserve oil fields have been depleted in the Cuu Long Basin (Thanh and Sugai 2021). In this basin, the marginal field is a potential candidate for new resources in Vietnam. However, high cost is a significant issue for us when attempting to develop a strategy to explore and develop the marginal field. To address this, 3D geo-cellular modeling has been adapted to deeply understand possible reserves (Islam et al. 2021). Furthermore, this modeling technique provides the target reservoir's better manner, such as faults, sub-layers, and the amount of oil reserves in the field (Mike 2009).

Moreover, 3D geo-cellular modeling was used to develop a new method by integrating artificial neural networks (ANNs) and geostatistical methods for static and dynamic CO₂ storage in the Nam Vang field, offshore Vietnam (Thanh et al. 2020). Therefore, this study adopts 3D geo-cellular modeling to explore the oil reserve in one of the marginal fields in offshore Vietnam. The geological model of the Lower Oligocene reservoirs of this field was constructed in this study using the interpretation of

✉ Hung Vo Thanh
vothanhhung198090@gmail.com;
vothanhhung1990@snu.ac.kr

¹ School of Earth and Environmental Sciences, Seoul National University, 1 Gwanak-ro, Gwanak-gu, Seoul 08826, South Korea

3D seismic acquisition and data from wells drilled in the field, such as TL-1X, TL-2X, and TL-3X. The present geological model aims to gather all available data to build a comprehensive geostatic representation of the Lower Oligocene reservoirs for a marginal field in offshore Vietnam. For the study, the marginal field was divided into two main zones based on two defined reservoir units (Thanh et al. 2020). They are zone E10 from top E10 to base E10 and zone E20 from top E20 to base E20. Generally, structural maps and faults from acquired 3D seismic data are used to generate structural and stratigraphic frameworks. Due to data availability, the stochastic approach was used to model facies and petrophysical properties (Al-khalifa et al. 2007; Cherpeau et al. 2010). Stochastic algorithms use random seed and input data and provide details of the results with differences (Xin et al. 2016).

Moreover, stochastic modeling is more complex than deterministic modeling and takes much longer to run. This indicates more aspects of the input data, specifically its variability (Thornton et al. 2018). This means that particular cells will appear in the results that are not driven by the input data and whose location is purely an artifact of the random seed used (Perevertailo et al. 2015). Therefore, the results will have a distribution that is more typical of the real case, although the specific variations are unlikely to match (Ailleres et al. 2019). This can be useful, particularly when taking the model to the simulation stage, as the variability of a property is likely to be just as important as it is the average value (Kamali et al. 2013). The disadvantage is that some crucial aspects of the model may be random. Therefore, a proper uncertainty analysis is performed with several realizations of the same property (Matias et al. 2015).

Furthermore, it is necessary to model the lithology before distributing the petrophysical properties of the 3D model. Several methods can be used for facies modeling. However, SIS has been recognized as the most valuable and flexible method for lithofacies modeling. In addition, SIS can predict the facies characteristics using well-log information to provide the facies distribution in uncore wells. This advantage is supported by stochastic facies modeling (Al-mudhafar 2017a).

Moreover, SIS has also been used to quantify geological uncertainties in modeling the architecture of complex reservoirs (Seifert and Jensen 1999). In addition, the SIS technique was employed to model the facies in sand-rich turbidite systems (Jordan and Goggin 1995). Most recently, SIS has been successfully adapted for lithofacies modeling in the Luhais oilfield in southern Iraq (Al-mudhafar 2021). In a similar study, SIS was considered in the development of an innovative carbonate facies modeling workflow in one of the UAE fields (Aidarbayev et al. 2020). A previous study demonstrated the advantage of SIS for lithofacies modeling. Therefore, in this study, SIS

was used to capture the depositional environment for clastic reservoirs in the marginal field regarding the lithofacies modeling.

The organization of this study is as follows: the field and geological description of the marginal field is outlined in Sect. 2, while Sect. 3 highlights the modeling framework for the paper. Section 4 presents the results and discussion of the modeling process. Finally, Sect. 5 presents the conclusions of the study.

Field and geological description

Field description

The Cuu Long Basin constitutes a Paleogene rift basin located off the southeast coast of Vietnam, covering approximately 150,000 km². It is separated from the Nam Con Son basin by the Con Son Swell in the southeast (Lee et al. 2001).

In the current tectonic sketch (Fig. 1), the Cuu Long Basin is situated southeast of the intra-continental plate that developed on the Eurasian continental crust. The Cuu Long Basin is a rift type, a subsided trough in the Paleogene that was founded on the cretaceous regressive continental crust. The Cuu Long Basin was filled with Neogene (N1²-Q) passive continental margin sediments. During the Cretaceous (J3-K), the region was occupied in the central part of a magmatic arc of a NE–SW trending from the adjacent continental area—from the Da Lat zone to Hainan Island in China. The Cuu Long Basin basement consists mainly of igneous magmatic arc (volcanic and intrusive) rocks (Dang et al. 2011b).

The tectonic evolution of the Cuu Long Basin can be divided into several main stages (Thanh and Sugai 2021):

1. Late Cretaceous–Eocene: Pre-rift uplift/initial rifting phase.
2. Late Eocene–Oligocene: Main rifting phase/initial ocean floor spreading phase. This led to the development of the main structural features within the basin, following extensional and transtensional deformations.
3. Early–Middle Miocene: Regional subsidence/renewed rifting. A change marked this from fault-controlled subsidence to thermally controlled, high-rate subsidence.
4. Late Miocene: Partial inversion/regional subsidence. During this stage, the entire area was dominated by compression in combination with the dextral strike-slip fault system in eastern offshore Vietnam, which probably generated basin uplift/partial inversion.
5. Pliocene–Pleistocene: Regional subsidence/renewed rifting. Diverse tectonic activity, from low to moderate amplitude differential uplift, acted across the basin.



Fig. 1 The study area is located in Cuu Long Basin modified from Thanh et al. 2020

Structurally, the Cuu Long rift basin is an elongated depression that is made up of a series of alternating horst, graben, and half-graben structural features arranged along the strike (the main strike is NE-SW) of the basin (Dang et al. 2011a). The location of the study area is shown in Fig. 1.

Facies and depositional environment

The facies and depositional environment analyses along the wells in the marginal field are based on petrographical analysis, core/cutting description, and log forms. The results of the sequence analyses are shown in Fig. 2. The details of the subsequence are summarized below.

Intra E20-basement subsequence

In this subsequence, the facies association is comprised of fine-grained facies—mudstone of lacustrine/floodplain, minor of very fine to fine sand facies of sheet flood and distal bar, and fine- to medium-grained sand facies of small channels. Regarding the depositional environment, this subsequence is a lacustrine, alluvial plain, and braided channel system. Fine-grained facies: mudstone is mainly deposited by suspension. Coarse-grained sediments were dominantly

divided from weathered granitoid provenance and rapidly deposited, close to the provenance.

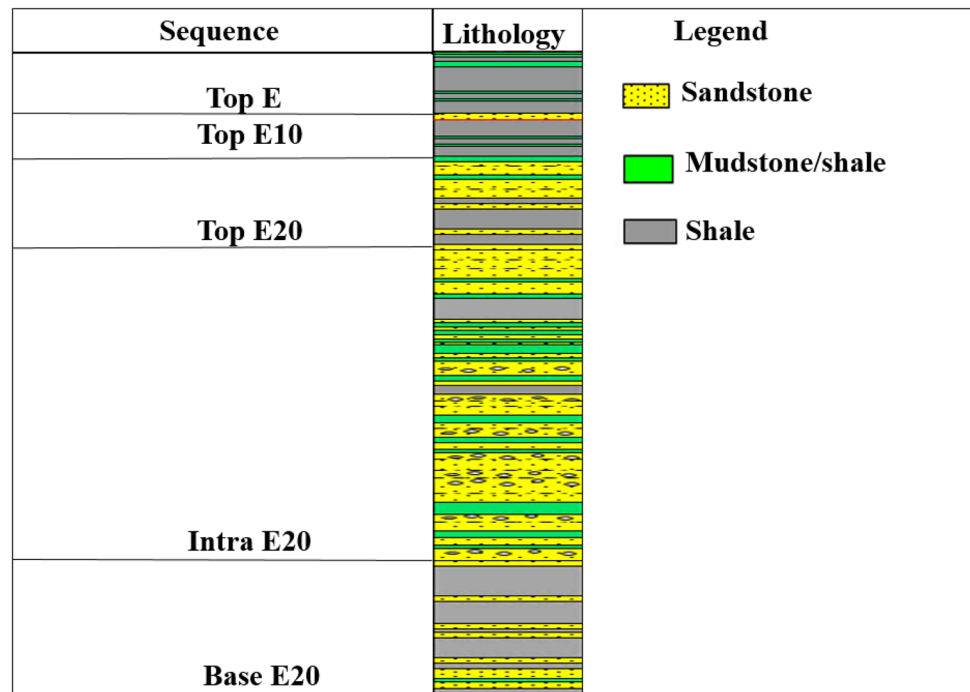
Top E20-intra E20 subsequence

The main facies of this subsequence is dominated by medium- to coarse-grained sand. Sand stacks of different facies, with various thicknesses, are often alternated and separated by thin mud beds or mud drapes. Individual sand bodies within the sand stacks are often separated by thin mud beds or mud drapes. These sand facies combined to form stacked sequences of 5 m up to 50 m thick, with gamma-ray logs representing a subtle cylinder shape. This subsequence was deposited in lacustrine and braided plains.

Top E10–Top E20 subsequence

This subsequence has very fine to fine sand facies, minor of very fine to fine sand facies, and low sand/shale ratio. In addition, fine-grained facies—mudstone—was mainly deposited by the suspension. Coarser-grained sediments were dominantly divided from weathered granitoid provenance and transported over a long distance and slowly deposited in a low-energy environment.

Fig. 2 The facies and depositional environment are highlighted for this study



Methodology

The data used for this research are the well-log data (porosity, permeability, and volume of clay), depth fault stick, depth surfaces, well markers, and oil–water contact data; more details will be introduced on each data type later. First, structural modeling was conducted for fault modeling, pillar girding, vertical layering, and contacts (Caumon et al. 2009). Property modeling is the process of filling the cells of the grid with petrophysical properties such as facies, porosity, permeability, and water saturation (Ali et al. 2020). Multiple geological realizations were conducted in the modeling process to reduce the geological uncertainty of the facies model (Al-mudhafar 2018). Thus, petrophysical models have also been generated according to each lithofacies realization (Al-mudhafar 2017b). Finally, the volumetric calculations for all realizations were calculated and ranked to determine the potential of oil reserves in the marginal field of the Cuu Long Basin, offshore Vietnam. Figure 3 illustrates the modeling loop used in this research.

Structural modeling

First, fault modeling is the initial step in the structure model process. Fault sticks were interpreted and imported into a geological package (Petrel Version 2012). Twelve fault stick sets were used for the fault modeling. In general, the Lower Oligocene faults were simple. Almost all fault systems are normal faults and fault orient in the NE–SW direction. Generally, fault modeling generates fault pillars, known as key

pillars, which define the slope and shape of the fault. There are up to five so-called shape points along each of these lines to adjust the form of the fault to match the input data perfectly. The key pillars are generated based on input data, such as depth fault sticks and structural maps (Islam et al. 2021).

Pillar girding was the next step in the structure model process. This process generates a 3D grid from the fault model. The grid is represented by pillars (coordinate lines) that define the possible positions for the grid block corner points. Thus, we can define directions along faults and borders to guide the girding process. The result from the pillar girding is the “Skeleton Framework”. The skeleton is a grid consisting of a top, middle, and base skeleton grid. The grid has no layers and only a set of pillars with the user given X and Y increments. For example, in the marginal Oligocene model, X and Y were set at $50\text{ m} \times 50\text{ m}$, and fault systems were made under force grid cells to be equally spaced along the faults. An illustration of the fault modeling and pillar girding is shown in Fig. 4.

The next step in 3D geo-cellular modeling is to create horizons and layering. The make-horizon process step is the first step in defining the vertical layering of the 3D grid in Petrel software version 2012 (Fig. 5). The vertical layering of the 3D grid is defined in two process steps: make the main reservoir layers (from seismic data) and make a vertical resolution (determined by cell thickness or several cell layers).

The depth surface data of the top E10, base E10, top E20, and base E20 in surface type were transferred to Petrel with well tops data. Using the Petrel Make Horizon module, these

Fig. 3. 3D geo-cellular modeling workflow is applied for this research (Thanh et al. 2020)

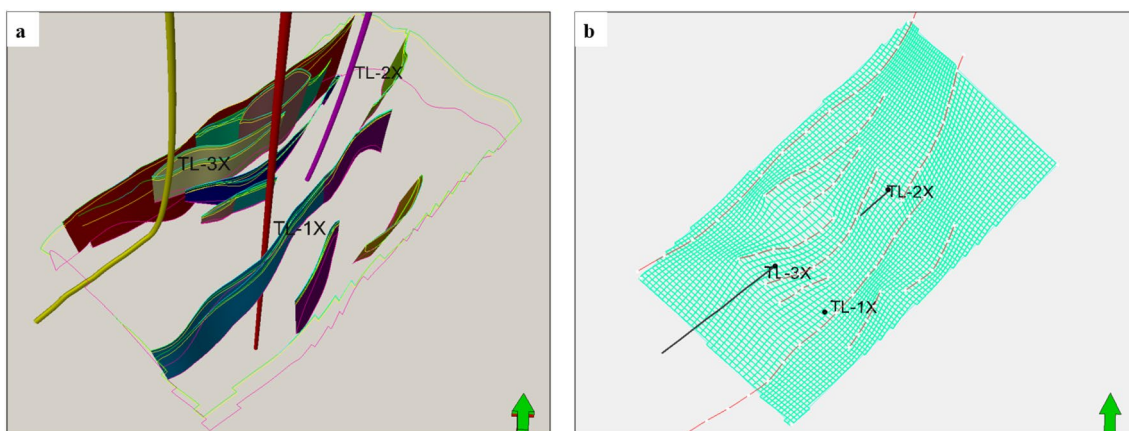
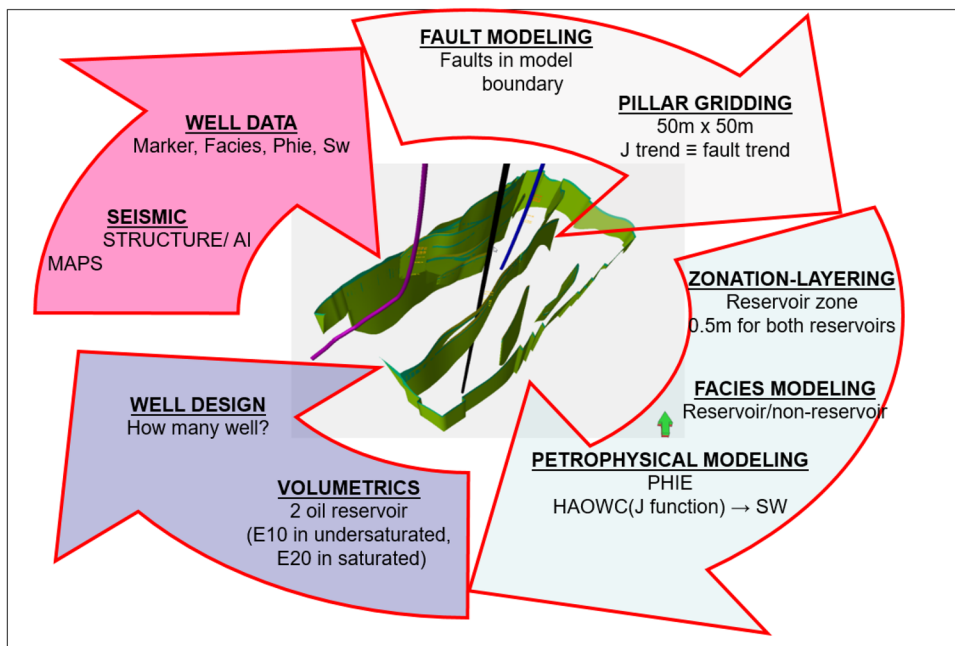


Fig. 4 The result of structural modeling is comprised of fault modeling (a) and pillar girding (b)

surfaces were used to create three zones, which combine with the fault system to construct a raw structural model or structural framework as “house of properties”. The geological horizon Top E10 is regarded as an erosion, while Base E10 and Top E20 are conformable. Base E20 is regarded as the base of the model.

The layering process is the last step in defining the vertical resolution of a 3D grid. The number of layers in each zone was considered to optimize the number of cells but was thin enough to capture the thinnest sand body. The layer modeling was focused on the main potential productive zones such as Zone E10 (Top E10 to Base E10) and Zone E20 (Top E20 to Base E20); the thickness of layers is 0.5 m. Under the scale of geological nature to be realized and runtime of the multiple simulations required, the grid

configuration was designed to optimize the number of cells and computing speed concerning reservoir heterogeneities. In general, the grid size and layering for the fine model are reasonable for representing the geometry and geological heterogeneities of the Oligocene reservoirs. Table 1 describes the information of the modeling parameters.

Property modeling

Property modeling involves filling grid cells with petrophysical properties such as facies, porosity, permeability, and water saturation. Therefore, these processes are dependent on the geometry of the existing grid. When interpolating between data points, the geological modeling process propagates property values along with the grid layers. The

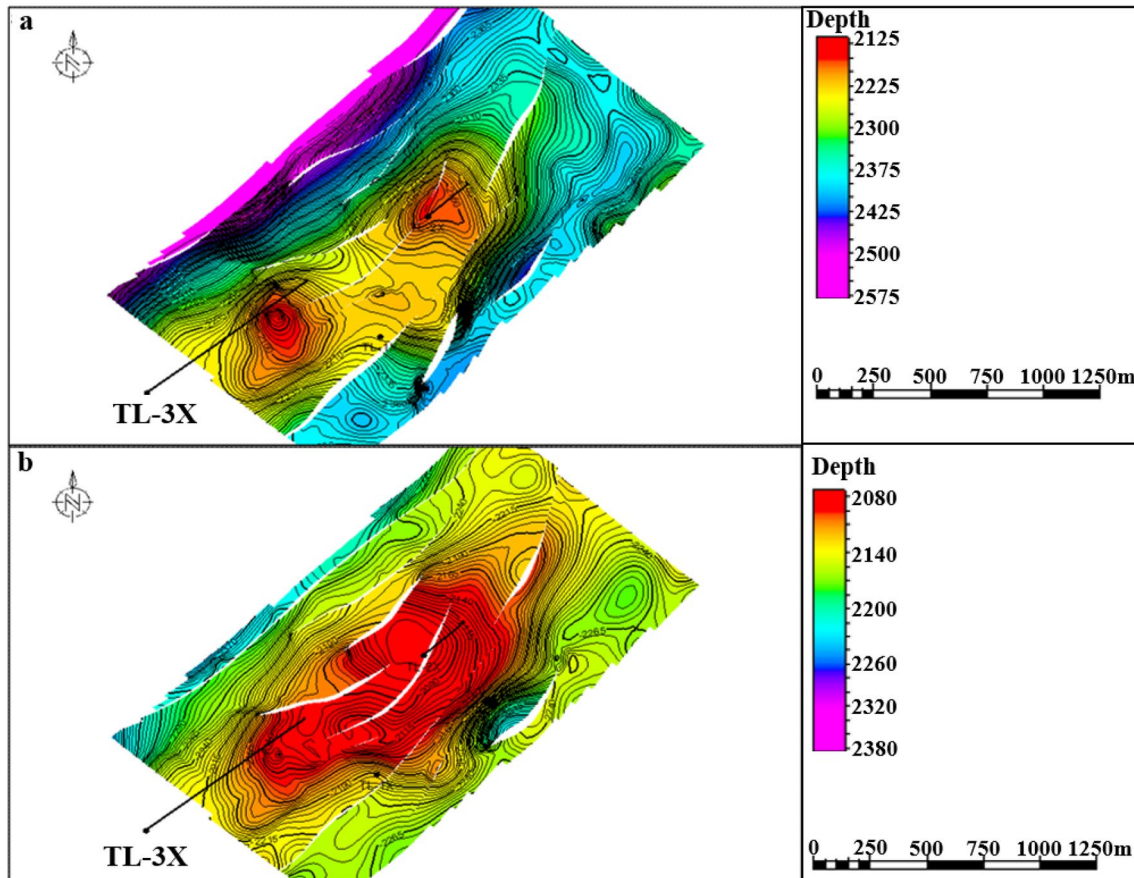


Fig. 5 The results of making horizon is based on Top E10 (a) and Base E20 (b)

Table 1 The variables of the modeling process

Parameters	Value
Cell size	50 m × 50 m
Zone	3 zones
Layer thickness	0.5 m
Number of layers	614 layers
Number of faults	12
Number of cells (I × J × K)	53 × 89 × 614 = 2,896,238

second period in building geological models is property modeling (He et al. 2020). The data input for property modeling includes well-log data (facies, porosity, permeability, volume of clay) and seismic trend maps. Property modeling in the marginal field is split into three separate stages (Zhong and Carr 2019):

- **Scale-up well logs:** The process of sampling values from well logs into the grid, ready for use as input to facies modeling and petrophysical modeling.
- **Data analysis:** The process of applying transformations to input data (normally upscaled well logs) identifies

trends and defines variograms describing the data. This is then used in the facies and petrophysical modeling to ensure that the same trends appear in the results.

- **Facies modeling:** Interpolation of discrete data, e.g., lithofacies.
- **Petrophysical modeling:** Interpolation of continuous data, for example, porosity, permeability, net to gross, and saturation.

Results and discussion

Scale-up well log

The facies was defined on base cases (such as reservoir/non-reservoir) as codes 1 and 0, respectively. These facies codes were created and applied for three wells based on volume shale and effective porosity cutoff of 0.35 and 0.09, respectively. Figures 6 and 7 illustrate the scale-up results of this study. Figure 6 presents the scale-up for different layer thicknesses for the E10 and E20 zones.

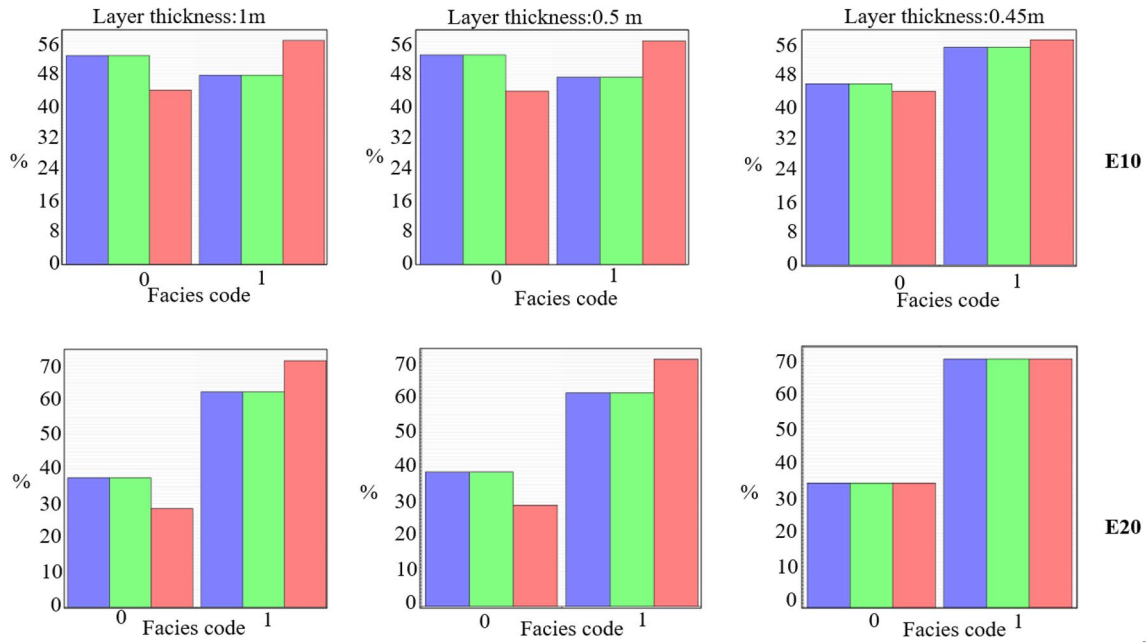


Fig. 6 Scale-up well-log facies is applied for modeling process

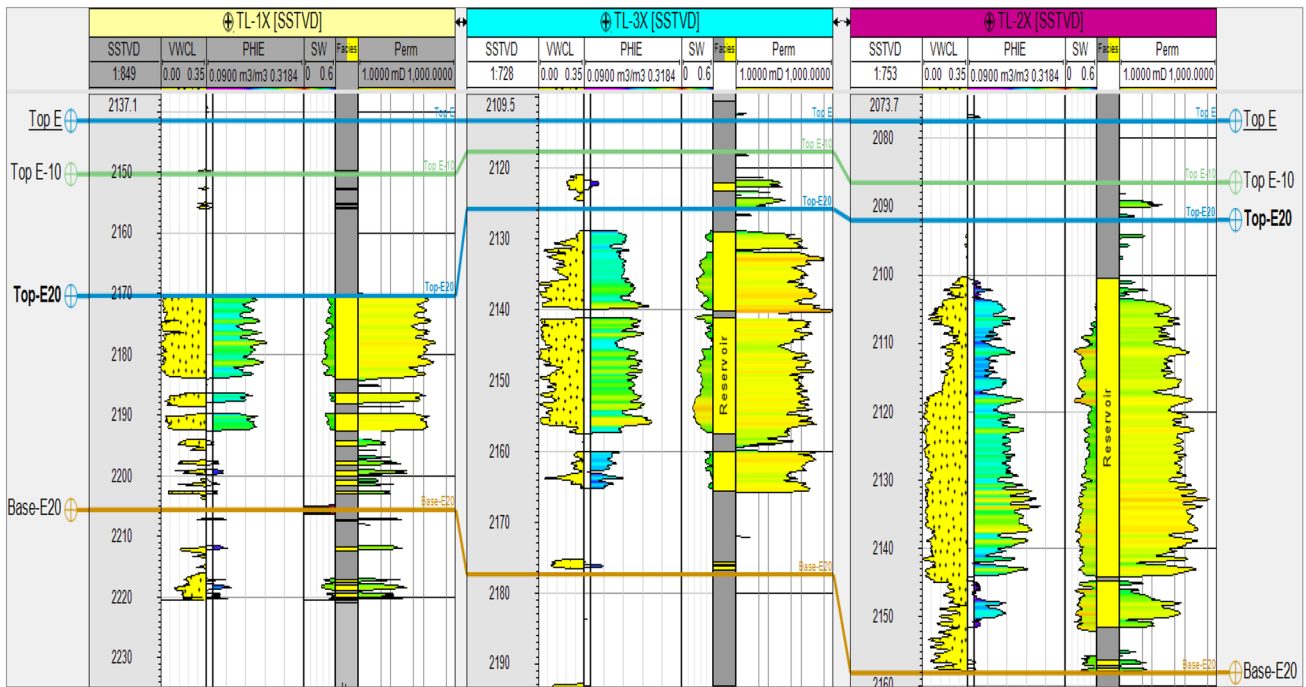


Fig. 7 Well cross section is mainly illustration with zones and facies

The layer thickness of 0.45 m is the best for both E10 and E20 reservoirs. Thus, this type of thickness will be utilized for the entire modeling process.

In addition, Fig. 7 illustrates the correlation between zones (E10, E20) and facies classification. As shown in this

figure, the reservoir facies are yellow, and the non-facies are represented by the brown color.

Data analysis

The data analysis process (DAP) of applying transformations to input data (normally upscaled well logs) identifies trends and defines variograms describing the data (Gringarten and Deutsch 1999). The DAP can be accessed from the process diagram and performs a detailed property analysis. In addition, depending on whether a property is discrete (e.g., facies) or continuous (e.g., porosity and permeability), we can analyze the facies proportion, thickness, calibration between continuous properties (e.g., sampled seismic), and facies within each zone and create a variogram of the discrete property. The DAP settings defined for discrete properties are saved for the current property and are accessed directly during facies modeling. Moreover, the continuous property can be defined by data transformations and generate variograms in the main, minor, and vertical directions.

In addition, data transformation enables the user to make the data stationary and standard normally distributed, which are requirements of many of the standard geostatistical algorithms (Gringarten and Deutsch 1999). After the scale-up well-log process, the data analysis tool was applied to analyze the facies proportion and thickness and create a variogram model (Gringarten and Deutsch 1999). Owing to constraints on the number of exploration/appraisal wells in the marginal field, the variogram model was created only for the vertical direction. The horizontal variogram was created based on the compressional wave velocity to shear wave velocity (V_p/V_s) variogram maps. The results of the facies

and porosity data analysis are shown in Figs. 8, 9, 10, and 11.

Facies model

Facies modeling is a means of distributing discrete facies throughout the model grid (Radwan 2021). We usually have upscaled well logs with discrete properties into the model grid and possibly defined trends within the reservoir by analyzing this data analysis process. In this research, the “Sequence Indicator Simulation” (SIS) method was applied to build the facies model (Seifert and Jensen 1999). The SIS method allows a stochastic distribution of the property using a predefined histogram. In addition, directional settings such as variograms and extensional trends were also honored. Based on the facies analysis results in Fig. 12, these results provide the facies volume proportion (histogram analysis), facies thickness distribution, and variation.

In the volume proportion, the probability curves were fitted from the original facies proportion at the well. The variogram was also checked carefully for each zone in the primary, minor, and vertical directions. To evaluate the geological uncertainty of the facies model, 20 geological realizations of facies distributions were created for the facies model. Then, the best one was selected to capture reservoir heterogeneity. Figure 13 represents the generation realizations and cross sections for the facies model of the E10 reservoirs. As shown in Fig. 12a, the effects of geological realizations were explored in this study. The

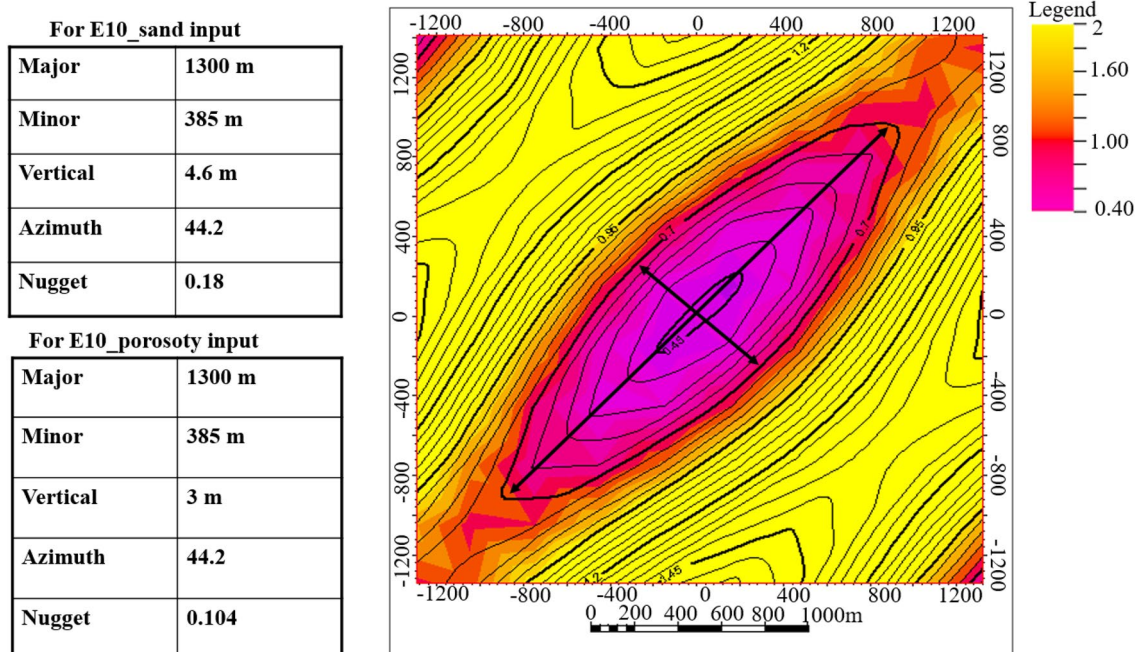


Fig. 8 V_p/V_s variogram map is utilized for E10 reservoirs

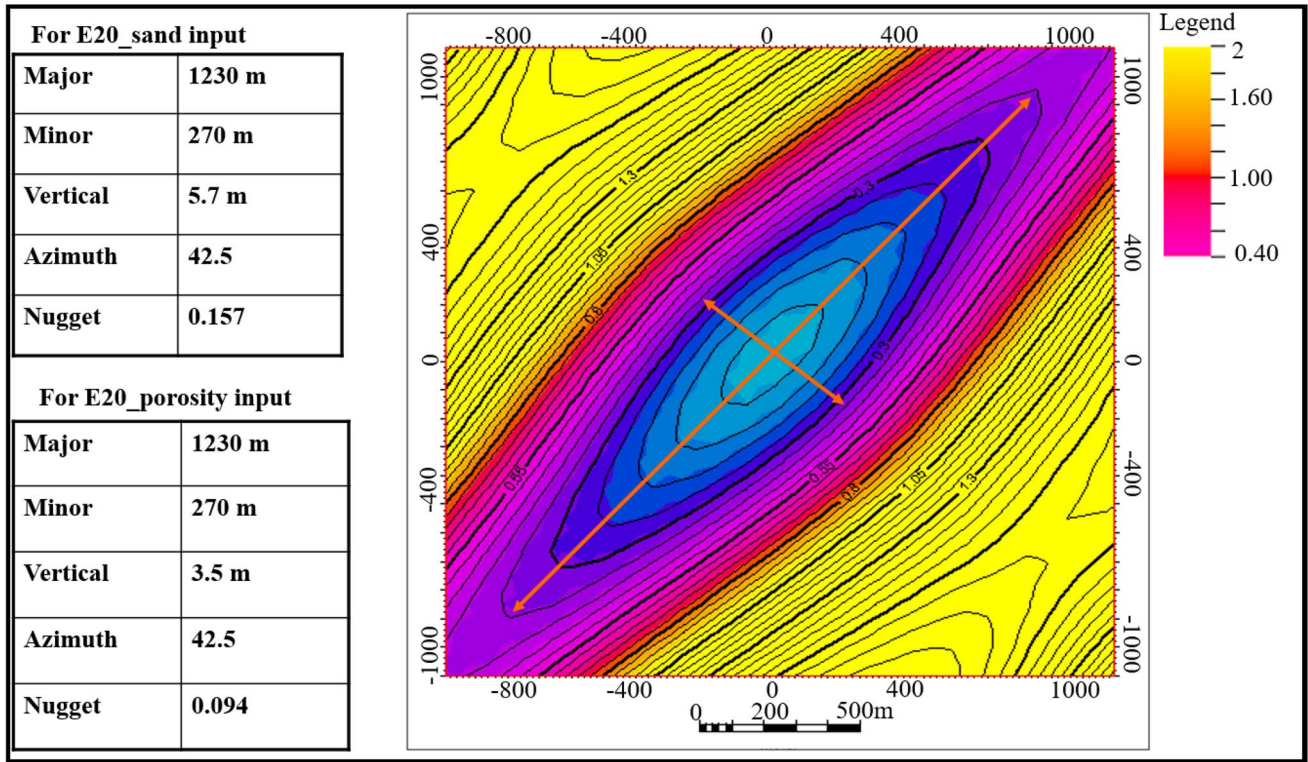


Fig. 9 Vp/Vs variogram map is utilized for E20 reservoirs

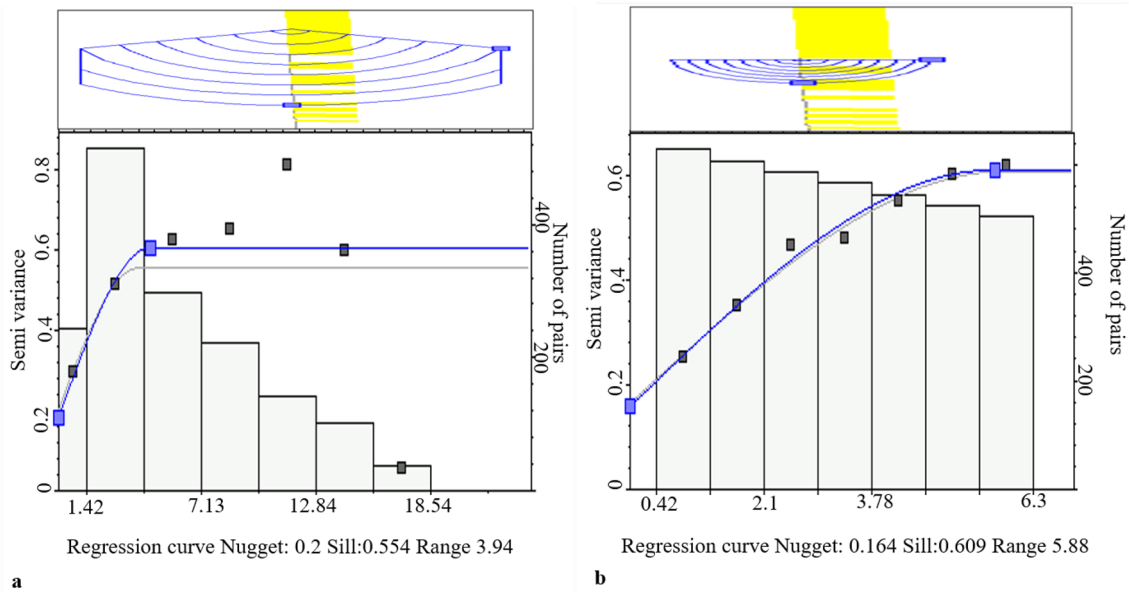


Fig. 10 Data analysis is considered for facies in E10 (a) and E20 (b) reservoirs

consistent case of facies was chosen to capture the characterization of the geosystem. Uncertainty would occur in geological modeling because the subsurface data are not easy to obtain. Nevertheless, geological modeling is an

excellent tool for deeply understanding the geology aspect. For better visualization, Fig. 12b depicts the cross section of the best facies model for E10 reservoir.

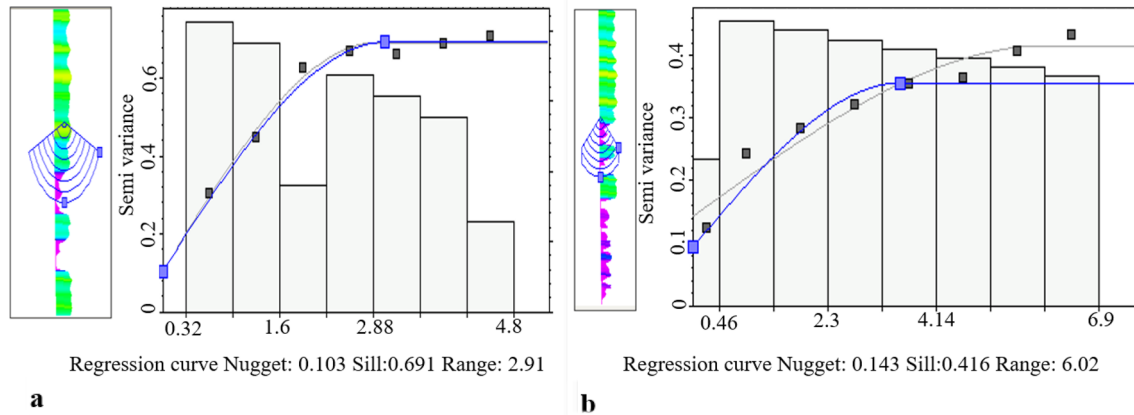


Fig. 11 Data analysis tool for E10 (a) and E20 (b) reservoirs

Similarly, the generation of facies realizations and cross sections for the E20 zone is shown in Fig. 13. As can be observed in this figure, the amount of sand distribution is higher than that in the E10 zone. Therefore, it seems that the E20 zone has more potential reserves than the E10 zone. In addition, the thickness of E20 is greater than that of the E10 reservoir. However, this is just a facies distribution that cannot determine which area is of interest for future development. Thus, the petrophysical modeling and volume calculation will be discussed in the next section.

Petrophysical modeling

Petrophysical results can be achieved in several ways, such as well-log interpolation (Attia et al. 2015; Abudeif et al. 2016a), petrographic image (Abudeif et al. 2016b), and petrophysical fingerprint techniques (Radwan et al. 2020). These techniques are useful for hydrocarbon-type detection in oilfields (Abudeif et al. 2018). Petrophysical interpretation is also helpful for classifying rock types during the waterflooding process in reservoirs (Radwan et al. 2021). However, petrophysical modeling is missing from these interesting works. Petrophysical modeling provides the distribution of porosity and permeability properties in the target field. Several steps to populate the model are required for the porosity (PHIE) modeling. First, the PHIE of each well-bore is derived from the log analysis result. Then, the PHIE was scaled up from the well log within the zones using the arithmetic average method. Next, the facies model is used as a filter to define the reservoir/non-reservoir in the PHIE model. The porosity values for all non-reservoir cells were always lower than the porosity cutoff value, whereas the porosity of all reservoir cells cannot be less than the cutoff value. Finally, PHIE modeling is run utilizing the sequential Gaussian simulation (SGS) method, variogram from data analysis, and standard distribution method from the upscaled

log distribution (Pyrcz and Deutsch 2014). In addition, SGS could provide an understanding of the geometry and continuity of petrophysical properties that have a direct impact on the reservoir flow behavior (Al-mudhafar 2021).

In this work, PHIE was upscaled bias to the chosen facies distribution, and 20 realizations were run.

Assuming that the porosity at well is the best and the well, the decreasing porosity so that the porosity distribution for the best case is chosen based on this assumption.

Figure 14 illustrates the porosity selection after the geological realizations. The best case is selected for the E10 reservoirs. The observation of this process shows that the porosity is consistent after the 17th realization. After this realization, the porosity distribution remains the same as in the 17th realizations. Regarding the E20 reservoirs, the selection of realization is similar to that of the E10 zone. The best-case porosity was achieved at the 20th realization. This scenario is shown to be the most consistent when compared to other realizations. Consequently, a deterministic method was applied to build the permeability model. Based on the porosity–permeability relationship provided from the core data of TL-3X, the permeability model is generated using the following equation:

$$\text{Perm}_{E10} = 2E - 05 * \text{pow}(\text{PHIE}, 5.0849) \quad (1)$$

$$\text{Perm}_{E20} = 3E - 08 * \text{pow}(\text{PHIE}, 7.8243) \quad (2)$$

The J function was applied to gather the water saturation spatial distribution within the reservoir grid for water saturation modeling. The J function was obtained from the core data of TL-3X. The functions are as follows:

$$\text{RQI}_{10} = \text{Sqrt}(\text{perm}_{10}/\text{PHIE}_{E10}) \quad (3)$$

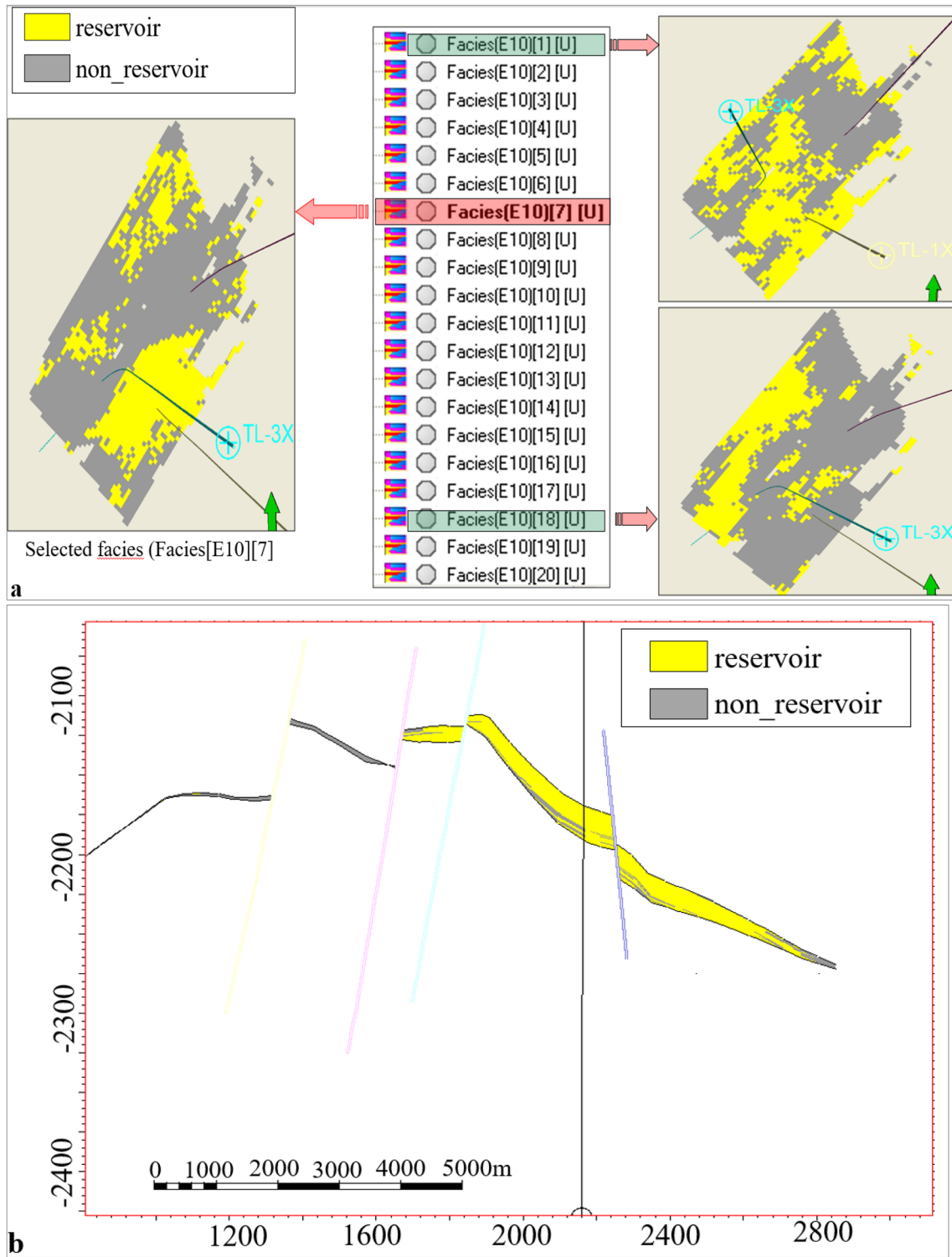


Fig. 12 The facies result is illustrated for E10 reservoirs. **(a)** Geological realizations generated to pick the consistent one. **(b)** Cross section of E10 facies model

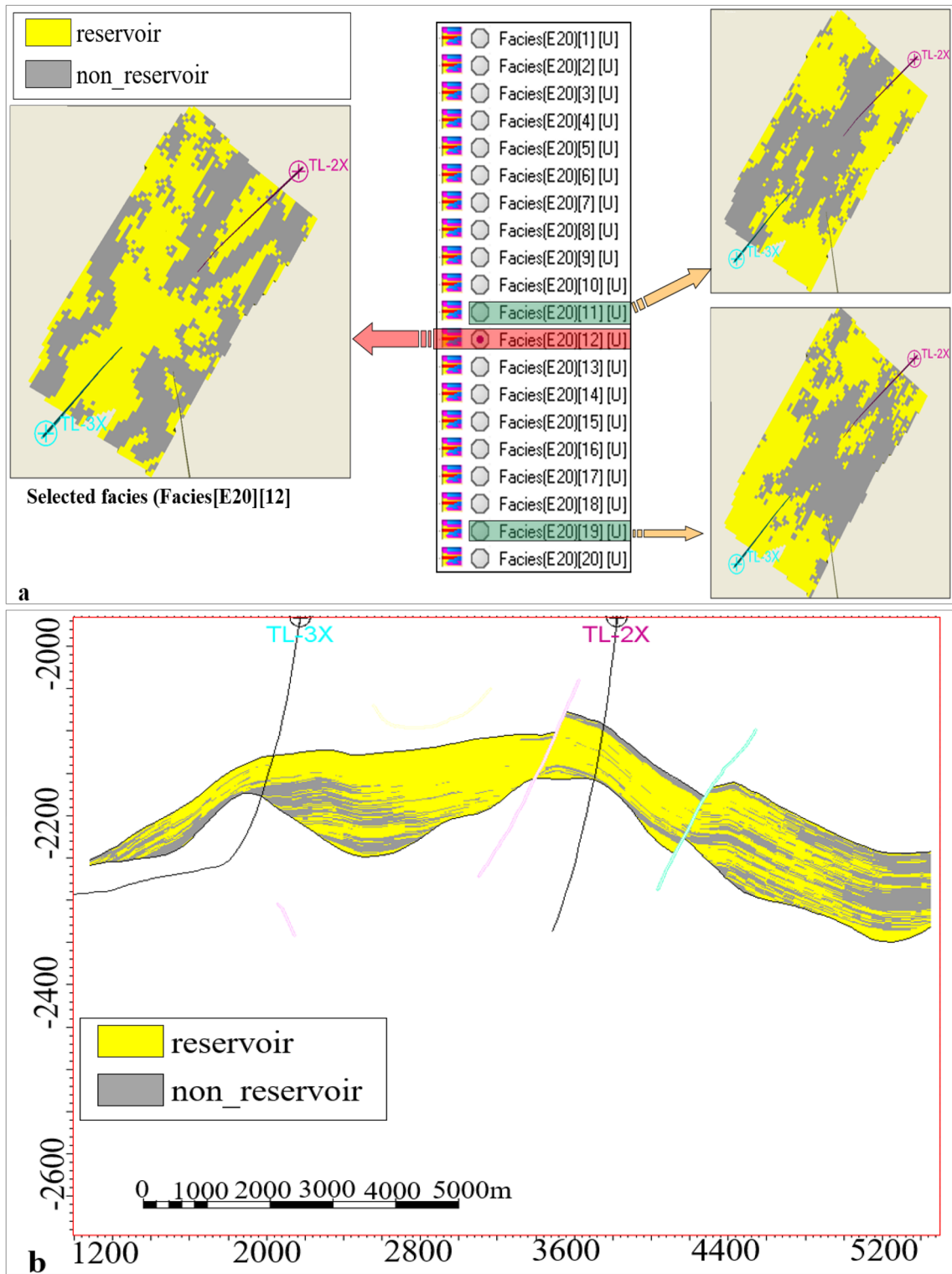


Fig. 13 The facies result is illustrated for E20 reservoirs. (a) Geological realizations generated to pick the consistent one. (b) Cross section of E20 facies model

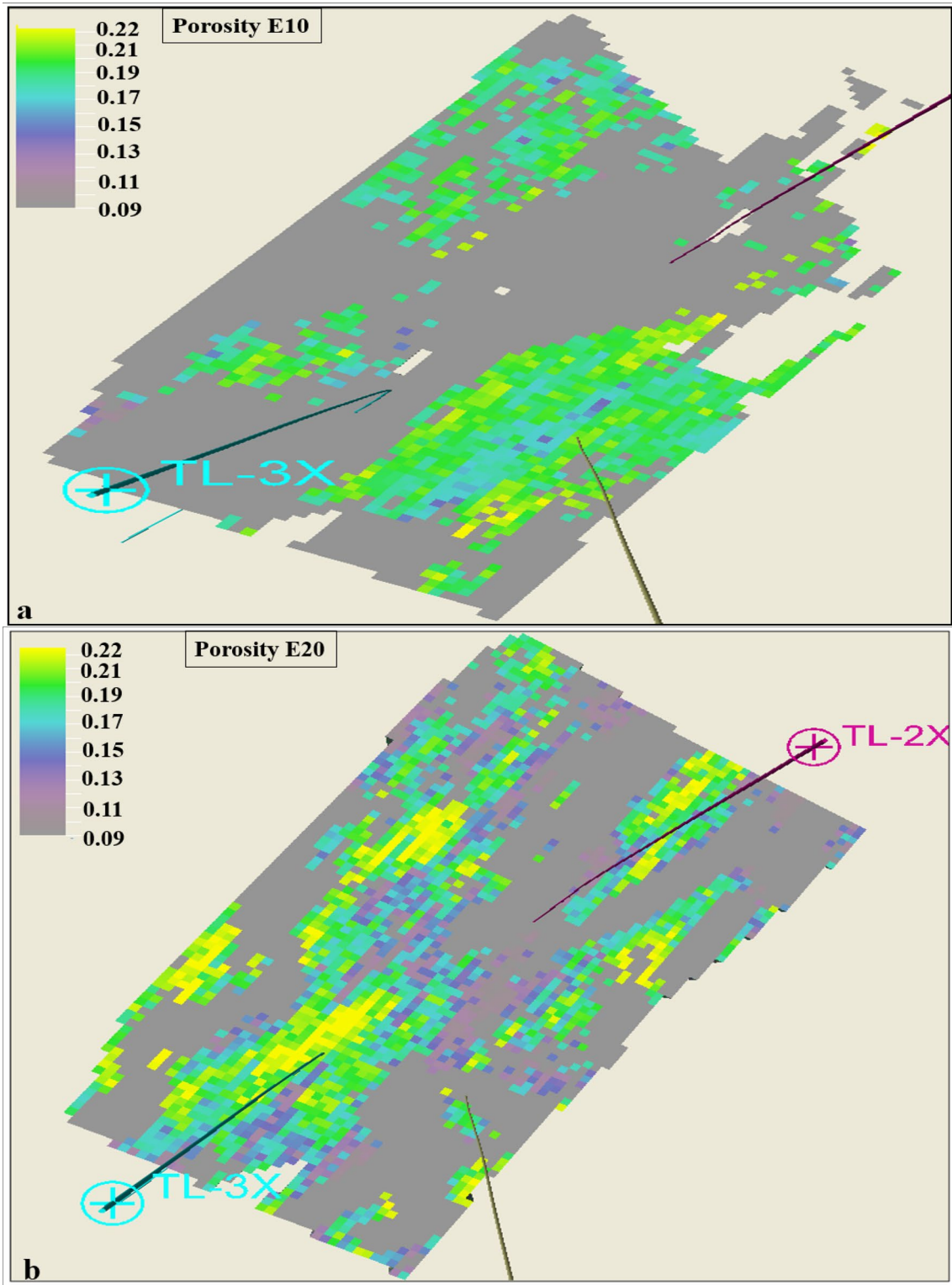


Fig. 14 Final porosity model is selected for E10 (a) and E20 (b) reservoirs

$$RQI_{20} = \text{Sqrt}(\text{perm}_{20}/PHIE_{E20}) \quad (4) \quad J_{\text{fun}}_{20} = (\text{Pc}_{20}/26.3) * RQI_{20} \quad (8)$$

$$\text{Pc}_{10} = (3.281 * (62.4 - 52.9) * \text{OWC}_H)/144 \quad (5) \quad \text{Sw}_{10} = 1.5975 * \text{pow}(J_{\text{fun}}_{10}, -0.383) \quad (9)$$

$$\text{Pc}_{20} = (3.281 * (62.4 - 49.1) * \text{OWC}_H)/144 \quad (6) \quad \text{Sw}_{20} = 2.0544 * \text{pow}(J_{\text{fun}}_{20}, -0.417) \quad (10)$$

$$J_{\text{fun}}_{10} = (\text{Pc}_{10}/26.3) * RQI_{10} \quad (7)$$

Figure 15a illustrates the permeability model using Eqs. (1) and (2). The co-kriging technique was used to

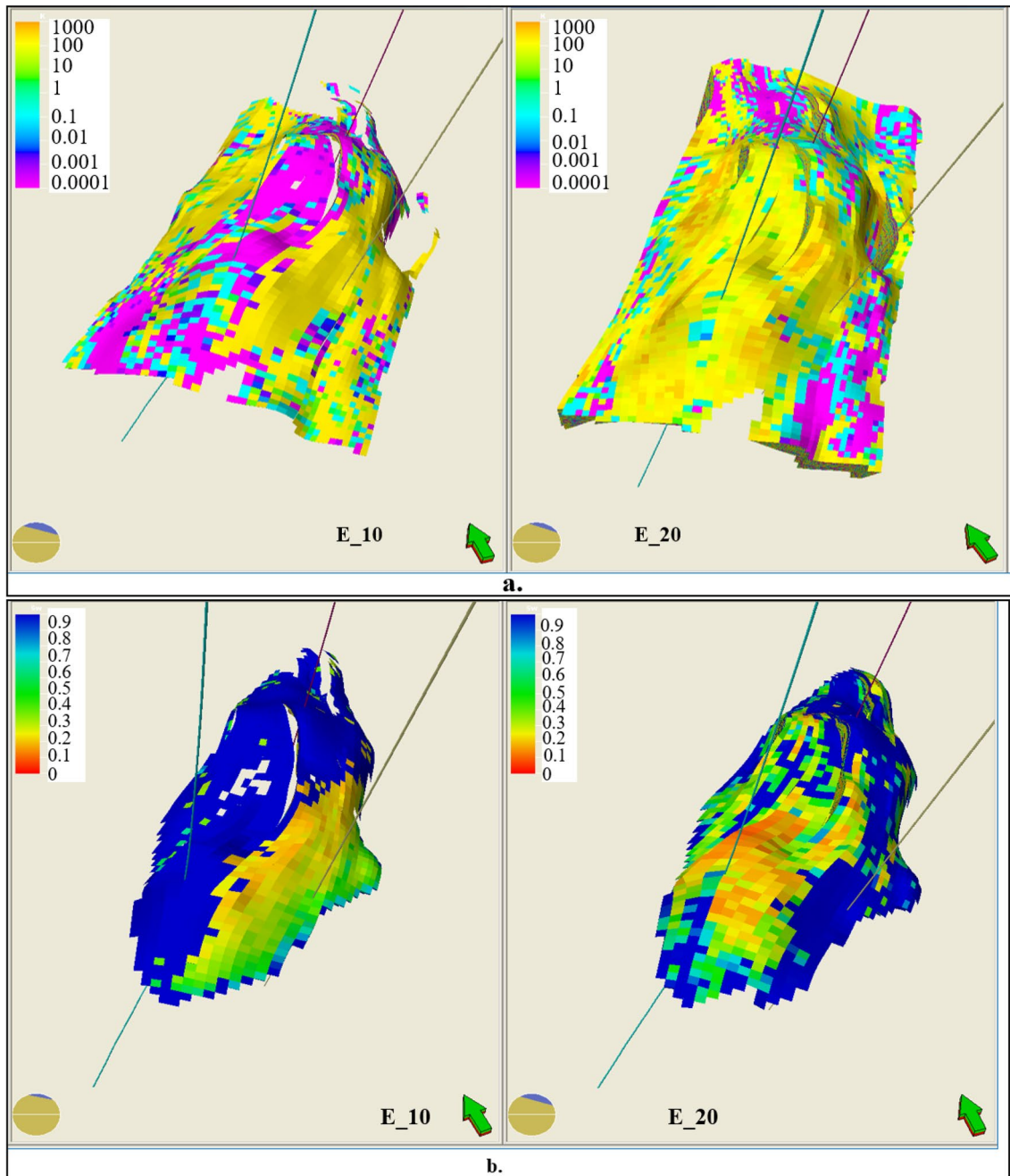


Fig. 15 The result modeling is highlighted for permeability (a) and water saturation (b) model for E10 and E20 reservoirs

distribute the 3D permeability model. Co-kriging could support the limitation of well data during the petrophysical modeling process (Thanh et al. 2020). This technique is a correlation factor between the primary and secondary data to calculate the distribution of the secondary variable at each point (Esmailzadeh et al. 2013). Thus, the co-kriging technique is suitable for the modeling process in this study. The illustration in Fig. 15a indicates that the target reservoir has a good distribution permeability in the marginal field. In addition, Fig. 15b presents the water saturation using the J function for both the E10 and E20 reservoirs.

Model verification

Data and model validations were performed at every significant modeling step. First, when data have been imported to the geological package (Petrel Version 2012), they should be under quality control (QC). Typical methods of data QC are to display them and to check statistics, histograms, etc. The QC process uses a general intersection to view the data in the cross section, and playing through the data set is an additional experience. Then, various cross sections were generated for QC, structural framework, facies modeling, and petrophysical modeling. Second, the skeleton grid was for quality control. The essential steps during QC also include checking for crossing pillars because possible negative cell

volumes are generated. Finally, the static method checks the matching between the input and output during the reservoir property modeling processes.

In addition, the synthetic data generated in a global well is a critical parameter for checking model quality. Depth synthetic information was used for comparison with the raw data to ensure no-depth mismatch. Synthetic data were also checked to ensure that the generated parameters matched the raw well data while generating facies and petrophysical realizations.

A statistical value check was also conducted to examine the facies volume proportion and trend to determine the matching status between generated realizations and input well data. Figures 16 represents histograms showing the facies and PHIE distribution of the input and output data

Table 2 The statistical analysis compares between raw well log and model results

Statistics	E10		E20	
	Raw log	Model	Raw log	Model
Min value	0	0	0	0
Max value	0.23	0.23	0.26	0.25
Mean value	0.11	0.12	0.14	0.13
Standard deviation	0.04	0.04	0.07	0.07

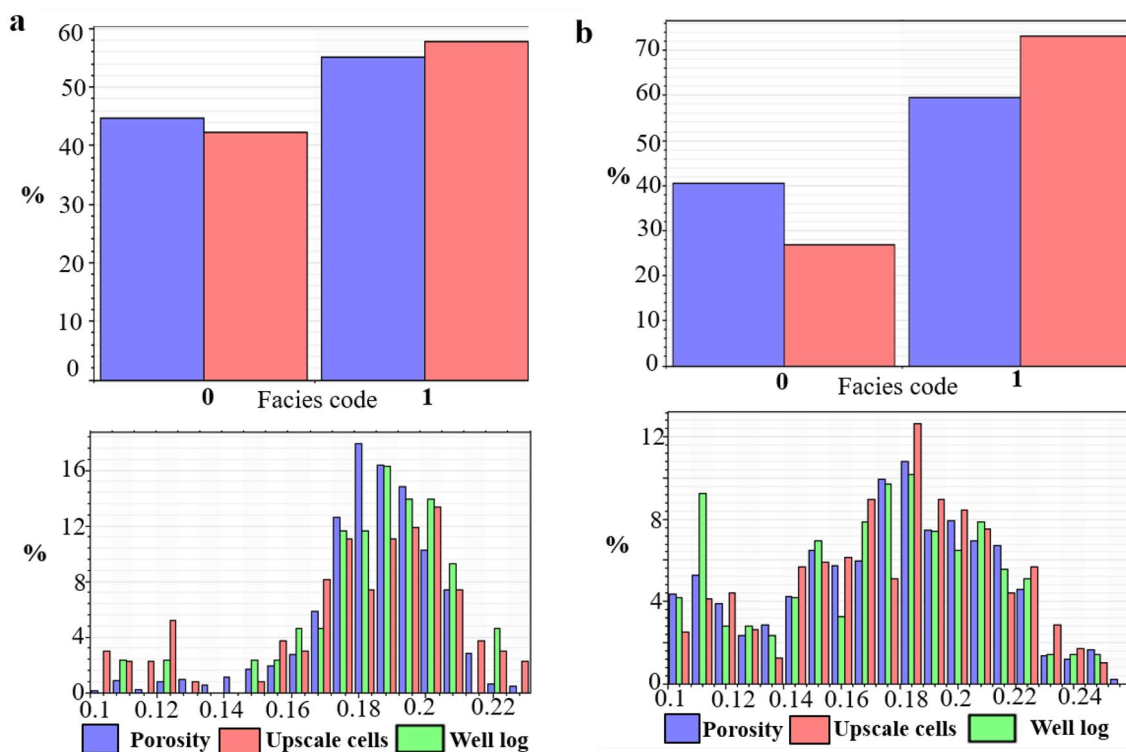


Fig. 16 Histogram analysis is obtained for facies and porosity in E10 reservoir (a) and E20 reservoir (b)

for zones E10 and E20. The visualization analysis from these histograms indicated an excellent model distribution for porosity in both the E10 and E20 reservoirs. In addition, the statistics of the two zones were also conducted for a better comparison. Table 2 shows the statistical analysis of the E10 and E20 reservoirs. Surprisingly, results were obtained between the raw log and 3D model. This indicates an excellent fit between the well-log and geo-cellular modeling approaches.

This result demonstrates that our model successfully represents the subsurface conditions for marginal fields in offshore Vietnam. The following section elaborates on the oil reserves for the E10 and E20 reservoirs for future development plans.

Volumetric calculation

The volumetric was computed based on the 3D geological reservoir model (Radwan and Chiarella 2021). Because of the facies definition, cutoff $V_{cl} < = 35\%$ and $PHIE > \geq 9\%$; therefore, the net to gross (NTG) was taken as 1. The NTG model was generated for volumetric calculation. In addition, the oil saturation (S_o), oil formation volume factor (B_o), and oil–water contact (OWC) were adapted from the Reserve and Resources Report (RAR) for the volumetric calculation. Volumetric sensitive processes were also carried out to choose the most appropriate OIIP value for the model (closer to the Conventional Volumetric Method shown in the latest RAR). The OIIP is calculated using the following equation (Petrel Software Manual 2012):

$$OIIP = BRV * NTG * PHIE * (1 - S_w) / B_o * C$$

To evaluate the uncertainty of the geo-cellular models, 200 cases were conducted for each reservoir. Figure 17 illustrates the volumetric calculations for the E10 and E20 reservoirs. The comparative results of the RAR and model calculations are shown in Table 3. There is a slight difference between the report and the model calculation. These results indicate that the proposed model is acceptable for further assessment.

Conclusion

This study applied geo-cellular modeling to evaluate the potential of reservoirs in the marginal field offshore. The following key points can be drawn from this research:

- As the maps of reservoirs are not being interpreted, the top and base maps of reservoirs generated from the top E and top basement lead to different volume reservoirs of rock in the Reserve and Resources Report and 3D model. Therefore, the structural model should be interpreted as a map of reservoirs calibrated with seismic attribute cubes.
- The facies model helps determine the sand distribution of reservoirs to support petrophysical modeling. This study used 20 facies geological realizations to reduce the geological uncertainty in porosity and permeability modeling. The porosity realization distributes the porosity properties for each facies realization.
- The petrophysical model was determined by a relationship adapted from the core analysis. Thus, deterministic modeling was used for permeability, while stochastic modeling was used to ensure the suitability of the target reservoirs.
- Sequential Gaussian simulation (SGS) was used for porosity realization to preserve the characteristics of the lithofacies model. In addition, the permeability distribution was adapted to the co-kriging technique to achieve the minimum variance of the estimation error in the modeling process.
- The volume of the reservoir rock is one of the critical factors that affect the oil's initial in-place calculation. It should be taken from the 3D model to eliminate the uncertainty.
- Geological uncertainty is necessary for 3D geo-cellular modeling in the exploration and production of hydrocarbons.
- This model provides the static geological model for future development plans by dynamic simulation

The potential oil reserve of the study reservoir was demonstrated using 3D geological modeling. However, uncertainties still exist in the Oligocene reservoir model for the marginal field. Some uncertainties are highlighted below:

- Structural maps are still unconfident due to the modeling process.
- While not yet studying the depositional conceptual model, the intermediate conceptual model has been referred to as for the assumption of direction, location, and size of geological feature distribution.
- Log upscaling and grid upscaling themselves lead to model uncertainty, particularly the hydrocarbon pore volume.

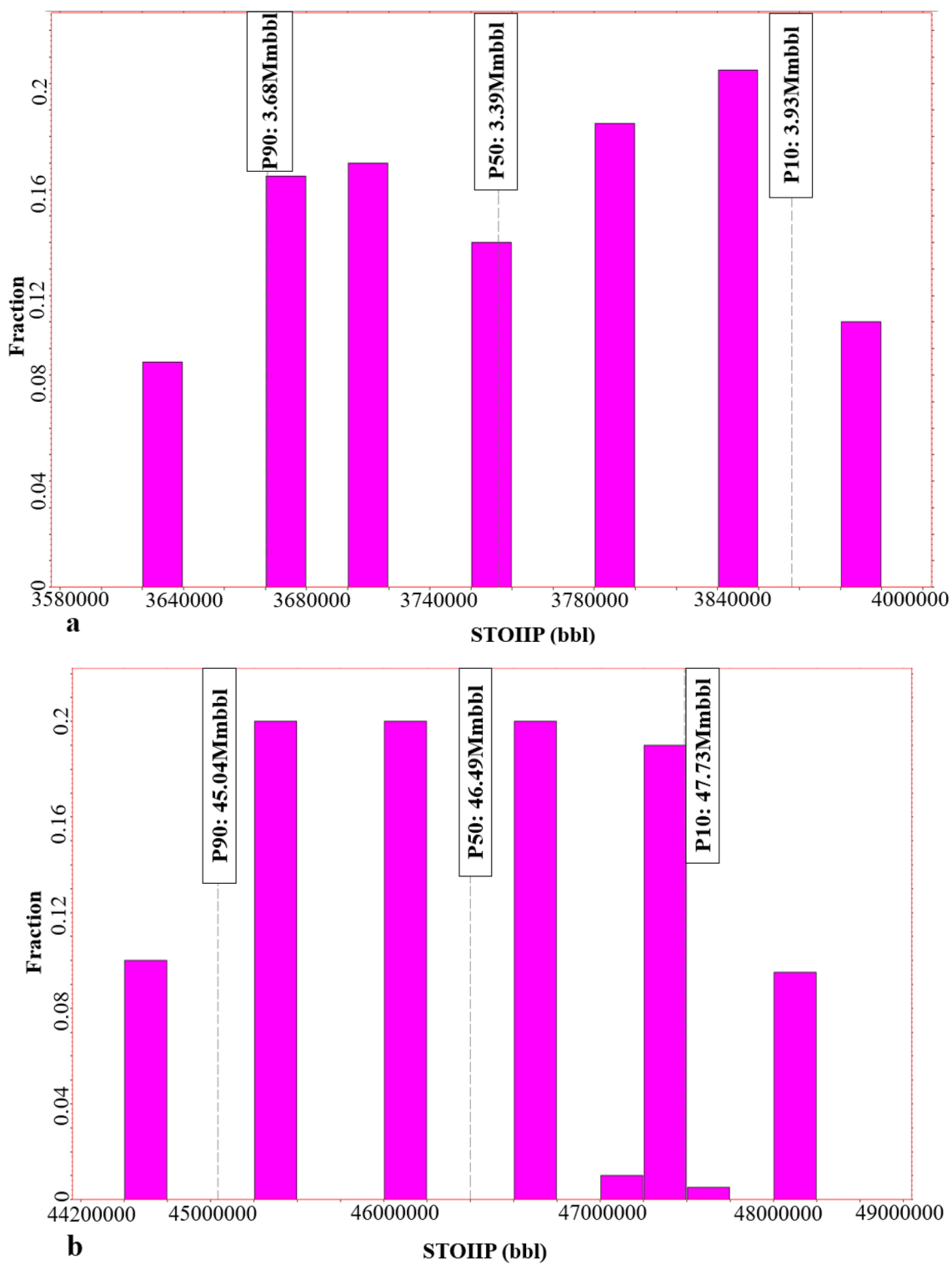


Fig. 17. Two hundred cases run for calculation the STOIP for E10 reservoir (a) and E20 reservoir (b)

Table 3 Results of volumetric obtained for this study

Reservoir	BRV 10 ⁶ m ³	OIIP from RAR (P50)	BRV 10 ⁶ m ³	OIIP from 3D (P50)
		Oil (MMbbl)		Oil (MMbbl)
E10	8.1	3.25	8.32	3.79
E20	270.5	46.88	190.42	46.49

Acknowledgements The authors would like to express their special gratitude to the BrainKorea21 (BK21) FOUR program for financial support.

Funding No funding was received for conducting this study.

Declarations

Conflict of interest The authors declare no conflict of interest.

Open Access This article is licensed under a Creative Commons Attribution 4.0 International License, which permits use, sharing, adaptation, distribution and reproduction in any medium or format, as long as you give appropriate credit to the original author(s) and the source, provide a link to the Creative Commons licence, and indicate if changes were made. The images or other third party material in this article are included in the article's Creative Commons licence, unless indicated otherwise in a credit line to the material. If material is not included in the article's Creative Commons licence and your intended use is not permitted by statutory regulation or exceeds the permitted use, you will need to obtain permission directly from the copyright holder. To view a copy of this licence, visit <http://creativecommons.org/licenses/by/4.0/>.

References

- Abudeif AM, Attia MM, Radwan AE (2016a) New simulation technique to estimate the hydrocarbon type for the two untested members of Belayim formation in the absence of pressure data, Badri field, Gulf of Suez, Egypt. Arab J Geosci. <https://doi.org/10.1007/s12517-015-2082-2>
- Abudeif AM, Attia MM, Radwan AE (2016b) Petrophysical and petrographic evaluation of Sidri member of Belayim formation, Badri field, Gulf of Suez, Egypt. J Afr Earth Sci 115:108–120. <https://doi.org/10.1016/j.jafrearsci.2015.11.028>
- Abudeif AM, Attia MM, Al-khashab HM, Radwan AE (2018) Hydrocarbon type detection using the synthetic logs: a case study, Baba member, Gulf of Suez, Egypt. J Afr Earth Sci 144:176–182. <https://doi.org/10.1016/j.jafrearsci.2018.04.017>
- Aidarbayev S, Pamungkas S, Dayyani TA et al (2020) An innovative carbonate facies modeling workflow that honors geological concept, case study of Thamama geological background regional depositional environment. In: Abu Dhabi international petroleum exhibition and conference. Abu Dhabi, UAE
- Ailleres L, Jessell M, De Kemp E et al (2019) Loop—enabling 3D stochastic geological modelling Loop—Enabling 3D stochastic geological modelling. In: AEGC 2019: from data to discovery. Perth, Australia, pp 1–3
- Ali M, Abdelmaksoud A, Essa MA et al (2020) 3D structural, facies and petrophysical modeling of C member of six hills formation, Komombo Basin, Upper Egypt. Nat Resour Res 29:2575–2597. <https://doi.org/10.1007/s11053-019-09583-5>
- Al-khalifa MA, Payenberg THD, Lang SC, Adelaide U (2007) Overcoming the challenges of building 3D stochastic reservoir models using conceptual geological models—a case study. In: 15th SPE Middle East oil and gas show and conference. Kingdom of Bahrain, pp 1–12
- Al-mudhafar WJ (2017a) Geostatistical lithofacies modeling of the upper sandstone member/Zubair formation in south Rumaila oil field, Iraq. Arab J Geosci. <https://doi.org/10.1007/s12517-017-2951-y>
- Al-mudhafar WJ (2017b) Multiple-point geostatistical lithofacies simulation of fluvial sand-rich depositional environment: a case study from Zubair formation/South Rumaila oil field. SPE Reserv Eval Eng 21:039–053. <https://doi.org/10.2118/187949-pa>
- Al-mudhafar WJ (2018) How is multiple-point geostatistics of lithofacies modeling assisting for fast history matching? A case study from a sand-rich fluvial depositional environment of Zubair formation in South Rumaila oil field. In: Offshore technology conference. Houston, Texas, USA, 30 April–3 May 2018
- Al-mudhafar WJ (2021) Geostatistical simulation of facies and petrophysical properties for heterogeneity modeling in a tidal depositional environment: a case study from upper shale member in a Southern Iraqi oil field. In: Unconventional resources technology conference. Houston, Texas, USA
- Attia MM, Abudeif AM, Radwan AE (2015) Petrophysical analysis and hydrocarbon potentialities of the untested Middle Miocene Sidri and Baba sandstone of Belayim formation, Badri field, Gulf of Suez, Egypt. J Afr Earth Sci 109:120–130. <https://doi.org/10.1016/j.jafrearsci.2015.05.020>
- Caumon G, Collon-Drouaillet P, de Veslud CLC et al (2009) Surface-based 3D modeling of geological structures. Math Geosci. <https://doi.org/10.1007/s11004-009-9244-2>
- Cherpeau N, Caumon G, Le'vy B, (2010) Stochastic simulations of fault networks in 3D structural modeling. Comptes Rendus Geosci 342:687–694. <https://doi.org/10.1016/j.crte.2010.04.008>
- Dang CTQ, Chen Z, Nguyen NTB et al (2011a) A successful story of integration geological characterization, reservoir simulation, assisted history matching and EOR in a giant fractured granite basement: a road map to maximize recovery in unconventional reservoirs. In: Offshore technology conference. Houston, Texas, USA, 2–5 May 2011, pp 1–12
- Dang CTQ, Chen Z, Nguyen NTB, Bae W (2011b) Improved oil recovery for fractured granite basement reservoirs: historical lessons, successful application, and possibility for improvement. In: SPE European formation damage conference. The Netherlands
- Esmailzadeh S, Afshari A, Motafakkerfard R (2013) Integrating artificial neural networks technique and geostatistical approaches for 3D geological reservoir porosity modeling with an example from one of Iran's oil fields. Pet Sci Technol 31:1175–1187. <https://doi.org/10.1080/10916466.2010.540617>
- Gringarten E, Deutsch CV (1999) Methodology for improved variogram interpretation and modeling for petroleum reservoir. In: Annual technical conference and exhibition. Houston, Texas, 3–6 October, pp 1–13
- He H, He J, Xiao J et al (2020) 3D geological modeling and engineering properties of shallow superficial deposits: a case study

- in Beijing, China. *Tunn Undergr Sp Technol* 100:103390. <https://doi.org/10.1016/j.tust.2020.103390>
- Islam A, Yungsi M, Qadri SMT et al (2021) Three-dimensional structural and petrophysical modeling for reservoir characterization of the Mangahewa formation, Pohokura gas-condensate field, Taranaki Basin, New Zealand. *Nat Resour Res* 30:371–394. <https://doi.org/10.1007/s11053-020-09744-x>
- Jordan DL, Goggin DJ (1995) An application of categorical indicator geostatistics for facies modeling in sand-rich turbidite systems, pp 781–792
- Kamali MR, Omidvar A, Kazemzadeh E (2013) 3D geostatistical modeling and uncertainty analysis in a carbonate reservoir, SW Iran. *J Geol Res* 2013:1–7
- Lee GH, Lee K, Watkins JS (2001) Geologic evolution of the Cuu Long and Nam Con Son basins, offshore Southern Vietnam, South China Sea. *Am Assoc Pet Geol Bull* 85:1055–1082
- Matias FV, Almeida JA, Chichorro M (2015) A multistep methodology for building a stochastic model of gold grades in the disseminated and complex deposit of Casas Novas in Alentejo, Southern Portugal. *Resour Geol* 65:361–374. <https://doi.org/10.1111/rge.12077>
- Mike S (2009) Oil field production geology. American Association of Petroleum Geologists Memoir, Tulsa
- Perevertailo T, Nedolivko N, Prisyazhnyuk O, Dolgaya T (2015) Application of geologic-mathematical 3D modeling for complex structure deposits by the example of lower-cretaceous period depositions in Western Ust—Balykh oil field (Khanty-Mansiysk autonomous district). *IOP Conf Ser Environ Sci*. <https://doi.org/10.1088/1755-1315/27/1/012016>
- Petrel Software Manual (2012) Schlumberger information solutions
- Pyrzc MJ, Deutsch CV (2014) Geostatistical reservoir modeling. Oxford University Press, Oxford
- Radwan AE (2021) Modeling the depositional environment of the sandstone reservoir in the middle Miocene Sidri member, Badri field, Gulf of Suez Basin, Egypt: integration of gamma-ray log patterns and petrographic characteristics of lithology. *Nat Resour Res* 30:431–449. <https://doi.org/10.1007/s11053-020-09757-6>
- Radwan AE, Chiarella D (2021) Combined stratigraphic-structural play characterization in hydrocarbon exploration: a case study of Middle Miocene sandstones, Gulf of Suez basin, Egypt. *J Asian Earth Sci*. <https://doi.org/10.1016/j.jseaes.2021.104686>
- Radwan AE, Abudeif AM, Attia MM (2020) Investigative petrophysical fingerprint technique using conventional and synthetic logs in siliciclastic reservoirs: a case study, Gulf of Suez basin, Egypt. *J Afr Earth Sci* 167:103868. <https://doi.org/10.1016/j.jafrearsci.2020.103868>
- Radwan AE, Nabawy BS, Kassem AA, Hussein WS (2021) Implementation of rock typing on waterflooding process during secondary recovery in oil reservoirs: a case study, El Morgan oil field, Gulf of Suez, Egypt. *Nat Resour Res* 30:1667–1696. <https://doi.org/10.1007/s11053-020-09806-0>
- Seifert D, Jensen JL (1999) Using sequential indicator simulation as a tool in reservoir description: issues and uncertainties. *Math Geol* 31:527–550
- Thanh HV, Sugai Y (2021) Integrated modelling framework for enhancement history matching in fluvial channel sandstone reservoirs. *Upstream Oil Gas Technol* 6:100027. <https://doi.org/10.1016/j.upstre.2020.100027>
- Thanh HV, Sugai Y, Nguele R, Sasaki K (2019) Integrated workflow in 3D geological model construction for evaluation of CO₂ storage capacity of a fractured basement reservoir in Cuu Long basin, Vietnam. *Int J Greenh Gas Control* 90:102826. <https://doi.org/10.1016/j.ijggc.2019.102826>
- Thanh HV, Sugai Y, Sasaki K (2020) Impact of a new geological modelling method on the enhancement of the CO₂ storage assessment of E sequence of Nam Vang field, offshore Vietnam. *Energy Sour Part A Recover Util Environ Eff* 42:1499–1512. <https://doi.org/10.1080/15567036.2019.1604865>
- Thornton JM, Mariethoz G, Brunner P (2018) Data descriptor: a 3D geological model of a structurally complex Alpine region as a basis for interdisciplinary research. *Sci Data* 5:1–20
- Xin C, Wei X, Li Y et al (2016) High-resolution seismic stochastic inversion as a direct input for reservoir modelling. In: Offshore technology conference this. Kuala Lumpur, Malaysia
- Zhong Z, Carr TR (2019) Geostatistical 3D geological model construction to estimate the capacity of commercial scale injection and storage of CO₂ in Jacksonburg-Stringtown oil field, West Virginia, USA. *Int J Greenh Gas Control* 80:61–75. <https://doi.org/10.1016/j.ijggc.2018.10.011>

Publisher's Note Springer Nature remains neutral with regard to jurisdictional claims in published maps and institutional affiliations.